

Physical validity of anisotropic models derived from isotropic fluid dynamics in $f(R, T)$ theory: An implication of gravitational decoupling

Tayyab Naseer^{1,2,*} and G. Mustafa^{3,†}

¹*Department of Mathematics and Statistics, The University of Lahore, 1-KM Defence Road Lahore-54000, Pakistan*

²*Research Center of Astrophysics and Cosmology, Khazar University,
Baku, AZ1096, 41 Mehseti Street, Azerbaijan*

³*Department of Physics, Zhejiang Normal University, Jinhua 321004, People's Republic of China*

In this paper, we derive multiple anisotropic analogs from the established isotropic model by means of the gravitational decoupling approach in a fluid-geometry interaction based theory. To accomplish this, we initially consider a static spherical perfect-fluid configuration and then introduce a new matter source to induce anisotropic behavior in the system. The resulting field equations encapsulate the entire matter distribution and thus become much complicated. We then split these equations into two sets through implementing a particular transformation, each set delineating characteristics attributed to their original fluid sources. We adopt the Heintzmann's ansatz and some constraints on extra gravitating source to deal with the first and second systems of equations, respectively. Furthermore, the two fundamental forms of the matching criteria are used to make the constant in the considered solution known. By utilizing the preliminary information of a star candidate LMC X-4, we assess the physical validity of the developed models. Our analysis indicates that both our models exhibit characteristics which are well-agreed with the acceptability criteria for certain parametric values.

Keywords: Heintzmann's model; Decoupling scheme; Anisotropic fluid; Stability.

I. INTRODUCTION

Recent discoveries in cosmology have challenged the traditional view of the structural configuration of astrophysical bodies existing in the universe. Instead of randomly distributed in space, they seem to exhibit systematic organization, which has captured the attention of researchers. The in-depth examination of interstellar objects has emerged as a central focus for astronomers aiming to unravel the enigma behind what we are known with as the accelerated expanding phenomenon. Dark energy is a mysterious force that appears to be driving this expansion, counteracting the pull of gravity. The discovery of dark energy in the late 1990s, through observations of distant supernovae, was initially met with skepticism but has since been independently confirmed. Dark energy is estimated to make up around 68-72% of the total energy and matter content of the universe, far exceeding the contributions of normal matter and dark matter. While general relativity (GR) can explain the expansion of the universe to some extent, it struggles to account for the cosmological constant associated with dark energy. This has led scientists to propose various extensions to GR in an attempt to better understand the nature of dark energy.

A direct extension within the realm of GR is the $f(R)$ theory, which stands as a notable progression in theoretical physics. This theory presents a deviation from the conventional Einstein-Hilbert action by exchanging the functions of the Ricci scalar R and its corresponding generic function. Noteworthy for yielding encouraging outcomes, this theoretical framework has been effectively utilized in the examination of compact stellar systems [1]-[5]. In a study by Astashenok and his colleagues [6], they explored the maximum mass limit of stars. Their results suggested that one of the components in the event GW190814 must be either a fast rotating neutron star or a massive black hole, effectively eliminating the possibility of it being a strange star. The existing literature highlights several significant works [7, 8]. Bertolami et al. [9] initially investigated the interaction between fluid and geometry within the $f(R)$ context. They accomplished this by combining the matter Lagrangian density and R into a single function. This concept has prompted scientists to focus their discussions on the subject of expanding cosmos [10].

Following this, Harko and co-researchers [11] extended this idea to the level of action, introducing a novel extension of GR, known as the $f(R, T)$ theory. In this framework, the interplay between geometry and the distribution of matter is mediated through R and trace of the energy-momentum tensor (EMT). This function gives rise to a non-

*Electronic address: tayyabnaseer48@yahoo.com

†Electronic address: gmustafa3828@gmail.com

conservative phenomenon, leading to the emergence of the additional force (see detail in [12]) within the field produced by an object, compelling test particles to deviate from geodesic trajectories. The research conducted by Houndjo [13] utilized a minimal gravity model to successfully explain the transition from a matter-dominated era to a late-time accelerated cosmic phase. Among the various $f(R, T)$ models, the $R + 2\omega T$ model has gained significant attention in the literature as it develops physically feasible interiors. This model was taken into account by Das et al. [14] to explore a three-layers gravastar structure, each layer among them is corresponded by a different equation of state. Multiple studies have explored various stellar configurations in the same theory [15]-[25]. One key concept within this theory revolves around its consideration of quantum effects, which in turn open up possibilities for particle generation. This particular aspect carries significant importance in the realm of astrophysical investigations as it suggests a correlation between quantum principles and $f(R, T)$ gravity. Some important works in this regard are [26]-[29].

Studying anisotropic models in astrophysics is crucial because many astrophysical systems, such as neutron stars and other compact objects, exhibit non-uniform pressure distributions and matter densities, which cannot be accurately described by isotropic models. Anisotropy can arise due to various factors, including strong gravitational fields, rotation, and magnetic fields, leading to different physical behaviors that are essential for understanding the stability, structure, and evolution of these celestial bodies. By incorporating anisotropic models, researchers can gain insights into phenomena such as the maximum mass of neutron stars and the effects of pressure anisotropy on surface redshift and thermal properties. Gravitational decoupling plays a pivotal role in transforming isotropic fluid models into anisotropic ones by allowing for the introduction of additional matter sources or fields that interact differently with the existing fluid dynamics. This approach facilitates the derivation of new field equations that reflect the complexities of anisotropic behavior while maintaining a connection to the original isotropic framework. By employing transformations and ansatz like Heintzmann's, one can systematically explore how deviations from isotropy impact the overall dynamics and stability of stellar configurations. The ability to assess physical validity through observational data of any star candidate further enhances the relevance of these models in explaining real astrophysical phenomena. Thus, the study of anisotropic models not only enriches our understanding of cosmic structures but also provides a more accurate representation of the underlying physics governing these systems.

The standard cosmic model is predominantly founded on the principle of isotropy and homogeneity on a grand scale. Nevertheless, there are instances of pressure anisotropy observed at smaller scales [30]-[32]. Additionally, the configuration of compact entities ensures the existence of anisotropy and non-uniform fluid dispersion. This pressure asymmetry arises from variations in the radial and transverse directionally-dependent pressure. A group of elements exists that induces non-uniformity in the internal structure, including phenomena like phase transitions [33], neutron stars surrounded by intense Maxwell field [34], pion condensation [35], and various additional influences [36, 37]. An additional contributor to this non-uniformity is the gravitational impact stemming from tidal forces [38]. The uniformity of our cosmos has been investigated through the analysis of X-ray emissions originating from clusters of galaxies [39]. This approach was subsequently applied to large-scale structures, revealing a conclusion that the universe exhibits anisotropic properties [40]. The presence of pressure anisotropy is a crucial factor warranting further examination, as it influences various physical attributes such as gravitational redshift, mass, etc. within a celestial system.

Astrophysicists have been motivated to seek exact (or numerical) solutions for celestial structures described by non-linear equations of motion within GR or alternative theories. The significance of compact interiors lies in their ability to satisfy requisite conditions, which necessitates precise solutions. Various methodologies have been proposed to address this, with gravitational decoupling emerging as a technique used to discuss solutions featuring diverse sources such as shear, heat dissipation, anisotropy, and others. The genesis of this methodology stemmed from the observation that the field equations encompassing diverse sources can be disentangled into distinct sets, simplifying the process of solving each set independently. Ovalle [41] introduced the minimal geometric deformation (MGD) scheme, a recent innovation that offers compelling elements for constructing physically viable stellar solutions, which was extended in [42]. Additionally, Naseer [43] utilized this approach to obtain the charged geometry within the complexity-free framework.

Ovalle et al. [44] utilized a spherical isotropic model and extended it to the anisotropic form by employing the MGD approach, ensuring physical feasibility of the solution. In a related development, Sharif and Sadiq [45] further extended this technique to include charged configurations, developed two distinct anisotropic versions of the Krori-Barua solution and examined their stability. The extensions of multiple geometric solutions has been made which are based on $f(R)$ formulations [46]. By utilizing the Durgapal-Fuloria ansatz as a foundational isotropic reference, multiple physically significant anisotropic analogs have been obtained [47]. Various researchers have proposed extensions of isotropic solutions such as Heintzmann and Tolman VII, and demonstrated their stability within the specified parameter range [48, 49]. Researchers considered the axial spacetime and developed appropriate solutions that exhibit stability [50]. Similarly, we have derived charged/uncharged anisotropic analogs of the Krori-Barua spacetime within a theory possessing strong non-minimal coupling [51, 52].

We present two distinct models possessing anisotropy by extending the isotropic spacetime in this article. For this,

we incorporate additional fluid source which may gravitationally coupled to the primary source within the $f(R, T)$ theory. The subsequent lines highlights the organizational structure of this paper. It begins from the next section in which we discuss the foundational aspects of the modified theory and its corresponding field equations, focusing on the combined matter source. Some detail on MGD scheme and how it works is presented in section **III**. In section **IV**, we take into account the Heintzmann's solution and determine constants involved by this ansatz using junction conditions. Section **V** discusses specific conditions that must be met for the model to be physically acceptable. We present two novel anisotropic models and their graphical explanation in section **VI**. Finally, we provide a summary of our findings in the concluding section.

II. MODIFIED $f(R, T)$ FIELD EQUATIONS

The $f(R, T)$ theory and its implications in the context of gravitational decoupling can be achieved by modifying the Einstein-Hilbert action as [11]

$$I = \int \sqrt{-g} \left[\frac{f(R, T)}{16\pi} + L_m + \tau L_\Phi \right] d^4x, \quad (1)$$

in which L_m expresses the matter Lagrangian that could be isotropic, anisotropic, dissipative, etc. according to the scenario under discussion. Here, we induce the extra gravitating source with the seed source whose Lagrangian is indicated by L_Φ . The quantity τ is referred to the decoupling parameter, commanding the impact of extra source on the original gravitational field. The action (1), after some lengthy calculations, produce the following governing equations as

$$G_{\sigma\omega} = 8\pi T_{\sigma\omega}^{(\text{tot})}, \quad (2)$$

where the factors on left and right sides explain the geometrical structure and the fluid distribution in the celestial interior, respectively. We categorize the term $T_{\sigma\omega}^{(\text{tot})}$ as

$$T_{\sigma\omega}^{(\text{tot})} = T_{\sigma\omega}^{(\text{eff})} + \tau \Phi_{\sigma\omega} = \frac{1}{f_R} T_{\sigma\omega} + T_{\sigma\omega}^{(\text{cor})} + \tau \Phi_{\sigma\omega}. \quad (3)$$

Here,

- $\Phi_{\sigma\omega}$ indicates the extra matter source,
- $T_{\sigma\omega}$ and $T_{\sigma\omega}^{(\text{cor})}$ are usual EMT and corrections due to modification of gravity. These corrections are defined by

$$T_{\sigma\omega}^{(\text{cor})} = \frac{1}{8\pi f_R} \left[f_T T_{\sigma\omega} + \left\{ \frac{R}{2} \left(\frac{f}{R} - f_R \right) - L_m f_T \right\} g_{\sigma\omega} - (g_{\sigma\omega} \square - \nabla_\sigma \nabla_\omega) f_R + 2f_T g^{\zeta\beta} \frac{\partial^2 L_m}{\partial g^{\sigma\omega} \partial g^{\zeta\beta}} \right], \quad (4)$$

where $f_T = \frac{\partial f}{\partial T}$ and $f_R = \frac{\partial f}{\partial R}$. Furthermore, the D'Alembert operator \square is defined by $\square \equiv \frac{1}{\sqrt{-g}} \partial_\sigma (\sqrt{-g} g^{\sigma\omega} \partial_\omega)$ and we symbolize the covariant derivative by ∇_σ . Following recent literature regarding the compact stellar solutions, we choose $L_m = P$ in this case with P being the isotropic pressure.

The isotropic EMT describes a system where the energy and momentum densities are the same in all spatial directions. This is a crucial assumption in modeling the large-scale structure of the universe, which is observed to be approximately homogeneous and isotropic on the largest scales. This is given as follows

$$T_{\sigma\omega} = (\mu + P) U_\sigma U_\omega + P g_{\sigma\omega}, \quad (5)$$

where

- μ being the density of the fluid,
- U_σ is the four-velocity.

The field equations of this modified gravity theory have the following trace component as

$$2f + T(f_T + 1) - Rf_R - 3\nabla^\sigma \nabla_\sigma f_R - 4f_T L_m + 2f_T g^{\zeta\beta} g^{\sigma\omega} \frac{\partial^2 L_m}{\partial g^{\zeta\beta} \partial g^{\sigma\omega}} = 0.$$

It must be highlighted the connection between different theories of gravity under certain circumstances. For instance, vanishing coupling of matter with geometry leads these results to $f(R)$ framework. The non-null divergence of the $f(R, T)$ EMT indicates a departure from the conservation phenomenon, leading to the emergence of an additional force affecting the trajectories of test particles moving in their gravitational fields. We can write it mathematically as

$$\begin{aligned} \nabla^\sigma T_{\sigma\omega} = & \frac{f_T}{8\pi - f_T} \left[(g_{\sigma\omega} L_m - T_{\sigma\omega}) \nabla^\sigma \ln f_T - \frac{1}{2} g_{\zeta\beta} \nabla_\omega T^{\zeta\beta} \right. \\ & \left. - \frac{8\pi\tau}{f_T} \nabla^\sigma \Phi_{\sigma\omega} + \nabla^\sigma (g_{\sigma\omega} \mathcal{L}_m - 2\mathbb{T}_{\sigma\omega}) \right]. \end{aligned} \quad (6)$$

The spherical interior metric plays a crucial role in the study of compact objects like black holes and neutron stars, providing a mathematical framework to describe the internal structure of these astrophysical entities. This spacetime is represented by the line element given by

$$ds^2 = -e^{p_1} dt^2 + e^{p_2} dr^2 + r^2 (d\theta^2 + \sin^2 \theta d\phi^2), \quad (7)$$

where $p_1 = p_1(r)$ and $p_2 = p_2(r)$. The four-velocity defined earlier in Eq.(5) is now become

$$U_\sigma = -\delta_\sigma^0 e^{\frac{p_1}{2}} = (-e^{\frac{p_1}{2}}, 0, 0, 0). \quad (8)$$

Adopting specific models allows for more flexibility in describing the gravitational interactions and the cosmic evolution. Also, by doing so, we can construct solutions that are better able to match the observational data. Following is a minimal $f(R, T)$ model with a real-valued constant ϱ as

$$f(R, T) = f_1(R) + f_2(T) = R + 2\varrho T. \quad (9)$$

The reason behind choosing this linear model is that we shall apply the decoupling strategy in the next section, requiring the field equations to be in simplest form so that they can easily be handled. Using the inflation potentials in their work, Ashmita et al. [53] obtained some significant results and attempted to match them with the existing data. They came to the conclusion that their results are consistent only for a particular range of the model constant, i.e., $-0.37 < \varrho < 1.483$. Some other considerable works in this context are [54]-[56].

Using Eqs.(2), (7) and (9) together leads to the development of the field equations as

$$e^{-p_2} \left(\frac{p_2'}{r} - \frac{1}{r^2} \right) + \frac{1}{r^2} = 8\pi (\mu - \tau\Phi_0^0) + \varrho(3\mu - P), \quad (10)$$

$$e^{-p_2} \left(\frac{1}{r^2} + \frac{p_1'}{r} \right) - \frac{1}{r^2} = 8\pi (P + \tau\Phi_1^1) - \varrho(\mu - 3P), \quad (11)$$

$$\frac{e^{-p_2}}{4} \left[p_1'^2 - p_2'p_1' + 2p_1'' - \frac{2p_2'}{r} + \frac{2p_1'}{r} \right] = 8\pi (P + \tau\Phi_2^2) - \varrho(\mu - 3P), \quad (12)$$

along with the non-conservation equation (6) expressed by

$$\begin{aligned} \frac{dP}{dr} + \frac{p_1'}{2} (\mu + P) + \frac{\tau p_1'}{2} (\Phi_1^1 - \Phi_0^0) + \tau \frac{d\Phi_1^1}{dr} \\ + \frac{2\tau}{r} (\Phi_1^1 - \Phi_2^2) = -\frac{\varrho}{4\pi - \varrho} (\mu' - P'). \end{aligned} \quad (13)$$

Equation (13) describes that the sum of all internal/external forces acting on a celestial body must be null to maintain the equilibrium, thus it is necessarily needed to explore this phenomenon in the presence of correction terms. The solution to a set (10)-(12) become obscured due to high degrees of freedom, such as $(p_1, p_2, \mu, P, \Phi_0^0, \Phi_1^1, \Phi_2^2)$. In such cases, it becomes necessary to choose certain constraints to ensure a unique solution.

III. EXPLORING GRAVITATIONAL DECOUPLING VIA MGD

Since we discuss the need of a systematic scheme in the previous section, the gravitational decoupling strategy serves as a best candidate to deal with such problems [44]. This scheme helps to simplify the complicated field equations by transforming them into another reference frame. Its implementation can be done only if a new metric is considered as a perfect-fluid solution to Eqs.(10)-(12). We adopt it as

$$ds^2 = -e^{p_3(r)} dt^2 + \frac{1}{p_4(r)} dr^2 + r^2 (d\theta^2 + \sin^2 \theta d\phi^2). \quad (14)$$

The equations help to transform both metric components are expressed as

$$p_3 \rightarrow p_1 = p_3 + \tau d_1, \quad p_4 \rightarrow e^{-p_2} = p_4 + \tau d_2. \quad (15)$$

In two types of the decoupling technique [57, 58], we adopt the MGD scheme which ensures the transformation of only the radial metric component. Following this, the new form of Eq.(15) is

$$p_3 \rightarrow p_1 = p_3, \quad p_4 \rightarrow e^{-p_2} = p_4 + \tau d, \quad (16)$$

where $d = d(r)$. The beneficial point of these transformations is that they always preserve the spherical symmetry. We choose the MGD approach for the current study due to its effectiveness in addressing the complexities associated with gravitational decoupling in anisotropic models. There are many advantages of MGD discussed below.

- The MGD approach simplifies the process of obtaining exact solutions by focusing on minimal modifications to the geometric structure of spacetime. This makes it easier to derive anisotropic analogs from isotropic models without introducing unnecessary complications.
- The MGD provides a clear framework for interpreting the physical implications of the derived models, ensuring that the solutions remain consistent with known astrophysical phenomena.
- Since our study is rooted in fluid-geometry interactions, MGD aligns well with the underlying principles of fluid dynamics, facilitating a seamless transition from isotropic to anisotropic configurations.
- Alternative methods for gravitational decoupling often involve more complex transformations or assumptions that may not be necessary for our specific context. These methods can sometimes lead to solutions that are less physically intuitive or harder to interpret in terms of astrophysical applications.

Implementing the transformation (16) on Eqs.(10)-(12) split them form different choices of η . The first set where the effect of additional source is disappeared, i.e., $\tau = 0$, is obtained as

$$e^{-p_2} \left(\frac{p_2'}{r} - \frac{1}{r^2} \right) + \frac{1}{r^2} = 8\pi\mu + \varrho(3\mu - P), \quad (17)$$

$$e^{-p_2} \left(\frac{1}{r^2} + \frac{p_1'}{r} \right) - \frac{1}{r^2} = 8\pi P - \varrho(\mu - 3P), \quad (18)$$

$$\frac{e^{-p_2}}{4} \left[p_1'^2 - p_2' p_1' + 2p_1'' - \frac{2p_2'}{r} + \frac{2p_1'}{r} \right] = 8\pi P - \varrho(\mu - 3P). \quad (19)$$

It is enough to adopt first two equations from the above set to determine the fluid parameters in their explicit form defined by

$$\mu = \frac{e^{-p_2}}{8r^2(\varrho^2 + 6\pi\varrho + 8\pi^2)} \left[\varrho r p_1' + (3\varrho + 8\pi) r p_2' + 2(\varrho + 4\pi)(e^{p_2} - 1) \right], \quad (20)$$

$$P = \frac{e^{-p_2}}{8r^2(\varrho^2 + 6\pi\varrho + 8\pi^2)} \left[(3\varrho + 8\pi) r p_1' + \varrho r p_2' - 2(\varrho + 4\pi)(e^{p_2} - 1) \right]. \quad (21)$$

As the second set completely characterizing the extra fluid source is concerned, we find the following field equations

$$8\pi\Phi_0^0 = \frac{d'}{r} + \frac{d}{r^2}, \quad (22)$$

$$8\pi\Phi_1^1 = d \left(\frac{p_1'}{r} + \frac{1}{r^2} \right), \quad (23)$$

$$8\pi\Phi_2^2 = \frac{d}{4} \left(2p_1'' + p_1'^2 + \frac{2p_1'}{r} \right) + d' \left(\frac{p_1'}{4} + \frac{1}{2r} \right). \quad (24)$$

Another fact about MGD scheme is the conservation of both fluid setups independently, leading to the phenomenon of not exchanging the energy between them. Since there are four terms (μ, P, p_1, p_2) in Eqs.(20) and (21) which need to be calculated, we may consider an ansatz to deal with these equations. Further, the same number of unknowns $(d, \Phi_0^0, \Phi_1^1, \Phi_2^2)$ are present in Eqs.(22)-(24), a single constraint on Φ -sector is needed at a time. After adding the additional source, the new variables must be defined. This is done in the following

$$\hat{\mu} = \mu - \tau\Phi_0^0, \quad \hat{P}_r = P + \tau\Phi_1^1, \quad \hat{P}_t = P + \tau\Phi_2^2, \quad (25)$$

along with the total anisotropy given by

$$\hat{\Delta} = \hat{P}_t - \hat{P}_r = \tau(\Phi_2^2 - \Phi_1^1), \quad (26)$$

vanishes when $\tau = 0$. In other words, when the effects of the extra source are extracted, we are left with the initial perfect fluid distribution.

IV. HEINTZMANN'S SPACETIME AND JUNCTION CONDITIONS

We devote this section for the development of a unique solution to Eqs.(20) and (21). The need for a particular metric component based solution is already discussed earlier. Following this, a recent solution has been proposed in the literature that helps in exploring the physics of physically relevant stellar structures [59, 60]. This perfect solution has the form

$$e^{p_1(r)} = b_1^2 (b_2 r^2 + 1)^3, \quad (27)$$

$$e^{p_2(r)} = \frac{2 (b_2 r^2 + 1) \sqrt{4b_2 r^2 + 1}}{(2 - b_2 r^2) \sqrt{4b_2 r^2 + 1} - 3b_2 b_3 r^2}, \quad (28)$$

$$\begin{aligned} \mu = & \frac{3b_2}{4(\alpha + 2\pi)(\alpha + 4\pi)(b_2 r^2 + 1)^2 (4b_2 r^2 + 1)^{3/2}} [2(\alpha + 3\pi)b_3 + 2b_2 r^2 \\ & \times \{ (2\alpha + 9\pi)b_3 + (6\alpha + 13\pi)\sqrt{4b_2 r^2 + 1} \} + 3(\alpha + 2\pi)\sqrt{4b_2 r^2 + 1} \\ & + b_2^2 r^4 (8\pi\sqrt{4b_2 r^2 + 1} - 7\alpha b_3)], \end{aligned} \quad (29)$$

$$\begin{aligned} P = & \frac{-3b_2}{4(\alpha + 2\pi)(\alpha + 4\pi)(b_2 r^2 + 1)^2 (4b_2 r^2 + 1)^{3/2}} \left[2b_2 r^2 \{ (3\alpha + 11\pi)b_3 \right. \\ & - (5\alpha + 9\pi)\sqrt{4b_2 r^2 + 1} \} - 3(\alpha + 2\pi)\sqrt{4b_2 r^2 + 1} + b_2^2 r^4 \{ 7(3\alpha + 8\pi)b_3 \\ & \left. + 8(\alpha + 3\pi)\sqrt{4b_2 r^2 + 1} \} + 2\pi b_3 \right]. \end{aligned} \quad (30)$$

The advantage to utilize Heintzmann's ansatz in our analysis is based on several key factors that enhance the robustness and applicability of our results. They are described as

- This ansatz is well-established in the literature for modeling anisotropic stellar structures. Its previous successful applications provide a strong foundation for our work and lend credibility to our chosen methodology.
- This ansatz allows for a straightforward mathematical treatment of the field equations, making it easier to derive explicit solutions while ensuring that the resulting models retain essential physical characteristics.
- While Heintzmann's ansatz is specific, it does not significantly limit the generality of our findings. The solutions derived from this approach can be extended or modified by varying parameters or considering different forms of matter sources. This adaptability ensures that our results remain relevant across a range of astrophysical scenarios.

Equations (27) and (28) contain a triplet of constants (b_1, b_2, b_3) that needs to be known so that the graphical analysis can be performed later for our resulting solutions. To perform this analysis, some conditions on the spherical interface ($\Sigma : r = \bar{R}$) have been proposed, referred to the junction conditions. We need both interior and exterior metrics to use such conditions. The former metric has the form for components (27) and (28) as

$$ds_-^2 = b_1^2 (b_2 r^2 + 1)^3 dt^2 + \frac{2(b_2 r^2 + 1) \sqrt{4b_2 r^2 + 1}}{(2 - b_2 r^2) \sqrt{4b_2 r^2 + 1} - 3b_2 b_3 r^2} dr^2 + r^2 (d\theta^2 + \sin^2 \theta d\phi^2), \quad (31)$$

while the later metric is adopted as the Schwarzschild solution with total mass symbolized by \bar{M} given by

$$ds_+^2 = -\frac{r - 2\bar{M}}{r} dt^2 + \frac{r}{r - 2\bar{M}} dr^2 + r^2 (d\theta^2 + \sin^2 \theta d\phi^2). \quad (32)$$

According to continuity of the first fundamental form, the following expressions hold at the boundary as

$$g_{tt}^- \stackrel{\Sigma}{=} g_{tt}^+, \quad g_{rr}^- \stackrel{\Sigma}{=} g_{rr}^+,$$

resulting in when combined with Eqs.(31) and (32) as

$$\frac{\bar{R} - 2\bar{M}}{\bar{R}} = b_1^2 (b_2 \bar{R}^2 + 1)^3, \quad (33)$$

$$\frac{\bar{R}}{\bar{R} - 2\bar{M}} = \frac{2(b_2 \bar{R}^2 + 1) \sqrt{4b_2 \bar{R}^2 + 1}}{(2 - b_2 \bar{R}^2) \sqrt{4b_2 \bar{R}^2 + 1} - 3b_2 b_3 \bar{R}^2}. \quad (34)$$

Another constraint achieved from the second fundamental form is the disappearance of the pressure at the hypersurface, i.e., $P \stackrel{\Sigma}{=} 0$. This condition yields when used in Eq.(30) as

$$2b_2 \bar{R}^2 \{ (3\alpha + 11\pi)b_3 - (5\alpha + 9\pi) \sqrt{4b_2 \bar{R}^2 + 1} \} - 3(\alpha + 2\pi) \sqrt{4b_2 \bar{R}^2 + 1} + b_2^2 \bar{R}^4 \{ 7(3\alpha + 8\pi)b_3 + 8(\alpha + 3\pi) \sqrt{4b_2 \bar{R}^2 + 1} \} + 2\pi b_3 = 0. \quad (35)$$

We attempt to solve Eqs.(33)-(35) simultaneously to get three constants but find it not possible. Therefore, we consider b_2 as a free parameter and calculate the remaining quantities in terms of this factor by using Eqs.(33) and (35) as

$$b_1 = \sqrt{\frac{\bar{R} - 2\bar{M}}{b_2^3 \bar{R}^7 + 3b_2^2 \bar{R}^5 + 3b_2 \bar{R}^3 + \bar{R}}}, \quad (36)$$

$$b_3 = \frac{\sqrt{4b_2 \bar{R}^2 + 1} (3\rho - 8\rho b_2^2 \bar{R}^4 - 24\pi b_2^2 \bar{R}^4 + 10\rho b_2 \bar{R}^2 + 18\pi b_2 \bar{R}^2 + 6\pi)}{21\rho b_2^2 \bar{R}^4 + 56\pi b_2^2 \bar{R}^4 + 6\rho b_2 \bar{R}^2 + 22\pi b_2 \bar{R}^2 + 2\pi}. \quad (37)$$

TABLE I: Constant doublet (b_1, b_3) for $b_2 = 0.001 \text{ km}^{-2}$ corresponding to multiple choices of ρ .

ρ	0	0.2	0.4	0.6	0.8	1.0	1.2
b_1	0.718457	0.718457	0.718457	0.718457	0.718457	0.718457	0.718457
b_3	2.1283	2.1789	2.2286	2.2775	2.3256	2.3729	2.4194

TABLE II: Constant doublet (b_1, b_3) for $b_2 = 0.003 \text{ km}^{-2}$ corresponding to multiple choices of ρ .

ρ	0	0.2	0.4	0.6	0.8	1.0	1.2
b_1	0.598964	0.598964	0.598964	0.598964	0.598964	0.598964	0.598964
b_3	1.3145	1.3396	1.3639	1.3876	1.4105	1.4328	1.4545

TABLE III: Constant doublet (b_1, b_3) for $b_2 = 0.005 \text{ km}^{-2}$ corresponding to multiple choices of ρ .

ρ	0	0.2	0.4	0.6	0.8	1.0	1.2
b_1	0.509276	0.509276	0.509276	0.509276	0.509276	0.509276	0.509276
b_3	0.8888	0.9059	0.9223	0.9382	0.9536	0.9684	0.9828

For different values of b_2 and the model parameter, we find the two constants b_1 and b_3 in Tables **I-III**. Note that these numerical values are obtained by using the approximate mass and radius of a compact star LMC X-4 as $\bar{M} = 1.04 \pm 0.09 M_\odot$ and $\bar{R} = 8.301 \pm 0.2 km$ [61]. This star is a well-studied binary system that contains a neutron star, making it an ideal candidate for examining the physical properties of compact stars. Its characteristics, including its mass, radius, and behavior under various conditions, have been extensively documented in the literature. This wealth of observational data allows us to make informed comparisons between our theoretical models and the actual physical properties of LMC X-4. Moreover, this star exhibits significant variability in its X-ray emissions and has been associated with various astrophysical phenomena, such as pulsations and outbursts. These features provide a rich context for testing the implications of our derived models. We observe from these Tables that the term b_1 is independent of ρ , however, decreases with the rise in b_2 . On the other hand, the quantity b_3 is directly and inversely related with ρ and b_2 , respectively.

V. PHYSICAL REQUIREMENTS FOR A VIABLE STELLAR MODEL

The solution of the Einstein or modified equations of motion shall represent a physically existing compact interior only if it is consistent with multiple conditions regarding acceptability of that model. Such conditions have been suggested and interrogated in the scientific literature [62]-[64]. Some highlights can be found in the following.

- Preventing from the existence of singularities in geometric terms at any point in the interior is one of the basic pillar of the solution to be physically feasible. Hence, the metric components, we choose or find, must obey increasing profile w.r.t. r and no singular point should occur anywhere. To check this, we achieve the coefficients (27) and (28) for $r = 0$ as

$$e^{p_1(r)}|_{r=0} = b_1^2, \quad e^{p_2(r)}|_{r=0} = 1,$$

indicating non-singularity. Also, the first-order derivatives of the same components are

$$\begin{aligned} (e^{p_1(r)})' &= 6b_1^2 b_2 r (b_2 r^2 + 1)^2, \\ (e^{p_2(r)})' &= \frac{12b_2 r \{2b_2 r^2 (b_3 (1 - b_2 r^2) + 2\sqrt{4b_2 r^2 + 1}) + \sqrt{4b_2 r^2 + 1} + b_3\}}{\sqrt{4b_2 r^2 + 1} \{b_2 r^2 (\sqrt{4b_2 r^2 + 1} + 3b_3) - 2\sqrt{4b_2 r^2 + 1}\}^2}. \end{aligned}$$

It is obvious from above equations that when we substitute $r = 0$, both derivatives become null and negative, otherwise. This confirms that the metric potentials possess an increasing behavior. We also check this graphically, but not add their plots here.

- The energy density should be typically positive and finite throughout the stellar region. The radial/tangential pressures also exhibit positive and finite values within the compact star, with the tangential pressure often being different from the radial one, indicating the presence of anisotropy. Further, they all must be maximum and minimum at the stellar core and boundary, respectively.
- The spherical mass function is a crucial element to be discussed while studying compact stars. This is because this factor allows for the investigation of various physical characteristics, such as the surface redshift, gravitational lensing, etc. Its mathematical formula is [65]

$$\hat{m}(r) = \frac{1}{2} \int_0^{\bar{R}} \bar{r}^2 \mu d\bar{r}. \quad (38)$$

It is interesting to know the closeness of particles within a compact star to explore how dense it is. In other words, the compactness is equal to the mass-radius ratio, symbolically expresses as

$$\lambda(r) = \frac{\hat{m}(r)}{r}. \quad (39)$$

A research done by Buchdahl shows its upper limit in the case of spherical fluid distribution as $\frac{4}{9}$ [66]. Another factor, named the redshift (or surface redshift) can be defined in relation with the mass as

$$Z_{rs}(r) = \frac{1 - \sqrt{1 - 2\lambda(r)}}{\sqrt{1 - 2\lambda(r)}}. \quad (40)$$

Different studies have been done in order to explore its acceptable values inside a compact interior and it was observed to be not greater than 5.211 [67].

- The energy conditions play a crucial role in the study of compact stars as they provide essential constraints on the physical properties of these astrophysical objects. By validating such bounds, we can ensure the consistency of theoretical models with the fundamental principles of relativity and the behavior of matter under extreme gravitational conditions. They are, in this case, given by [68, 69]

$$\left. \begin{aligned} \hat{\mu} &\geq 0, & \hat{\mu} + \hat{P}_t &\geq 0, \\ \hat{\mu} + \hat{P}_r &\geq 0, & \hat{\mu} - \hat{P}_t &\geq 0, \\ \hat{\mu} - \hat{P}_r &\geq 0, & \hat{\mu} + 2\hat{P}_t + \hat{P}_r &\geq 0. \end{aligned} \right\} \quad (41)$$

- As the stability of massive systems is concerned, the models which fulfil stability criteria are more likely to be studied for further exploration. In this regard, the literature suggests multiple schemes that can be used to analyze whether a resulting model is stable or not. For example, the causality condition is a well-established way to do so [70]. According to this, the light's speed must be greater than that of the sound, i.e.,

$$0 < \hat{V}_t^2 = \frac{d\hat{P}_t}{d\hat{\mu}} < 1, \quad 0 < \hat{V}_r^2 = \frac{d\hat{P}_r}{d\hat{\mu}} < 1.$$

Further, cracking can occur in a compact star due to sensitivity of the radial forces to local density perturbations. This can cause the self-gravitating object to exhibit instability within certain ranges of some physical parameters. Hence, Herrera [71] suggested a condition that must be fulfilled to avoid the cracking as $0 < |\hat{V}_t^2 - \hat{V}_r^2| < 1$.

VI. MODELING ANISOTROPIC SOLUTIONS

This section deals with the solution of second set (22)-(24). For this, we use multiple constraints to make highly complicated differential equations easy to solve. The following subsections shall present different models and their physical acceptability.

A. Model 1: Density-like Constraint

To obtain the first model, we consider that the density of perfect fluid is equal to that of the additional source. This constraint has widely been employed in the literature while studying compact systems. In terms of mathematical symbols, we can write it as [72]

$$\mu = \Phi_0^0. \quad (42)$$

Equation (42) leads to a linear-order differential equation when we combine it with (20) and (23) as

$$\begin{aligned} &\frac{1}{8\pi} \left\{ \frac{d'(r)}{r} + \frac{d(r)}{r^2} \right\} - \frac{e^{-p_2}}{8r^2(\varrho^2 + 6\pi\varrho + 8\pi^2)} \\ &\times [\varrho r p_1' + (3\varrho + 8\pi) r p_2' + 2(\varrho + 4\pi)(e^{p_2} - 1)] = 0. \end{aligned} \quad (43)$$

Writing the above equation in terms of Heintzmann's potentials (27) and (28), we are left with

$$\begin{aligned} &\frac{1}{8\pi} \left\{ \frac{d'(r)}{r} + \frac{d(r)}{r^2} \right\} - \frac{3b_2}{4(\alpha + 2\pi)(\alpha + 4\pi)\psi^3(b_2r^2 + 1)^2} \left[3(\varrho + 2\pi)\psi + 2b_3 \right. \\ &\left. \times (\varrho + 3\pi) + b_2^2r^4(8\pi\psi - 7\varrho b_3) + 2b_2r^2\{(6\varrho + 13\pi)\psi + (2\varrho + 9\pi)b_3\} \right] = 0, \end{aligned} \quad (44)$$

where $\psi = \sqrt{4b_2r^2 + 1}$. We can find the term $d(r)$ from the above equation, either numerically or analytically. So we first attempt to calculate the exact solution and become able to achieve this. The obtained form for $d(r)$ is given by

$$d(r) = \frac{B_1}{r} + \frac{3\pi}{4(\varrho^2 + 6\pi\varrho + 8\pi^2)\sqrt{b_2}r} \left[\frac{2\sqrt{b_2}b_3r(\varrho + (7\varrho + 8\pi)b_2r^2)}{\psi(b_2r^2 + 1)} \right]$$

$$\begin{aligned}
& - \frac{4(3\varrho + 4\pi)\sqrt{b_2 r}}{b_2 r^2 + 1} + 4\sqrt{3}\varrho b_3 \tanh^{-1}\left(\frac{\sqrt{3}\sqrt{b_2 r}}{\psi}\right) + 16\pi\sqrt{b_2 r} \\
& - 7\varrho b_3 \sinh^{-1}(2\sqrt{b_2 r}) + 12\varrho \tan^{-1}(\sqrt{b_2 r}) \Big], \tag{45}
\end{aligned}$$

with an integration constant B_1 whose value must be taken as zero to avoid the singularity at $r = 0$. Further, the corresponding g_{rr} potential is determined using Eq.(16) as

$$\begin{aligned}
e^{p_2(r)} &= \frac{2(b_2 r^2 + 1)\sqrt{4b_2 r^2 + 1}}{(2 - b_2 r^2)\sqrt{4b_2 r^2 + 1} - 3b_2 b_3 r^2} + \frac{3\pi\tau}{4(\varrho^2 + 6\pi\varrho + 8\pi^2)\sqrt{b_2 r}} \\
&\times \left[\frac{2\sqrt{b_2} b_3 r(\varrho + (7\varrho + 8\pi)b_2 r^2)}{\psi(b_2 r^2 + 1)} - \frac{4(3\varrho + 4\pi)\sqrt{b_2 r}}{b_2 r^2 + 1} + 16\pi\sqrt{b_2 r} + 4\sqrt{3} \right. \\
&\times \left. \varrho b_3 \tanh^{-1}\left(\frac{\sqrt{3}b_2 r}{\psi}\right) - 7\varrho b_3 \sinh^{-1}(2\sqrt{b_2 r}) + 12\varrho \tan^{-1}(\sqrt{b_2 r}) \right]. \tag{46}
\end{aligned}$$

We can use this along with Eqs.(25) and (26) to find the final expressions of effective matter determinants. Certain characteristics corresponding to this developed model are now ready to be investigated in this modified gravity context. For this, we need to choose some parametric values so that the graphical analysis can be smoothly performed. In this regard, we adopt $\tau = 0.1, 0.2, 0.3$, $\varrho = 0.1, 0.6, 1.1$ and $b_2 = 0.005 \text{ km}^{-2}$ to observe how the considered minimal model (9) and decoupling strategy affect our results. Figure 1 shows the graphs of the deformation function (45) and modified potential (46) for all above parametric choices. Both plots show consistent data within their domains.

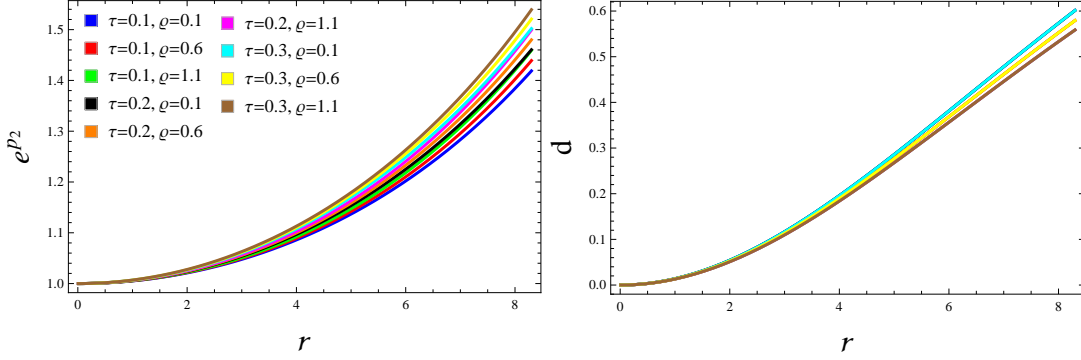


FIG. 1: Modified g_{rr} potential and deformation function for model 1.

We now put our focus on the behavior of effective physical parameters such as energy density, pressures in different directions and anisotropy. We plot all these factors in Figure 2 which show that the resulting model 1 can be of physical interest because it is compatible with the required trend. We observe the impact of density to be inversely proportional to both parameters ϱ and τ . However, both pressure ingredients show increasing and decreasing profile for the rise in τ and ϱ , respectively. Moreover, anisotropy should not be appeared at the core which is guaranteed from the last plot of Figure 2. Notice that the system with high difference between radial/tangential pressures is obtained for $\tau = 0.3$ and $\varrho = 0.1$. Some other physical factors depending on the mass are graphically shown in Figure 3, from which we find all of them to be acceptable. Rather than plotting the Misner-Sharp mass in geometric terms, we plot the mass in combination with the energy density. This is advantageous because we reach to the conclusion that the model becomes massive for $\tau = 0.1$ and $\varrho = 0.1$ as compared to the other values. The viability analysis is done in Figure 4, exhibiting positive trend of the matter-dependent factors, hence, model 1 is viable. The three plots of Figure 5 show the absence of cracking in the interior, implying that the solution is stable.

B. Model 2: Pressure-like Constraint

We now assume that the pressure of both perfect and additional fluid sources is equal to each other, leading to multiple physically feasible solutions. We express this as [73]

$$P = \Phi_1^1. \tag{47}$$

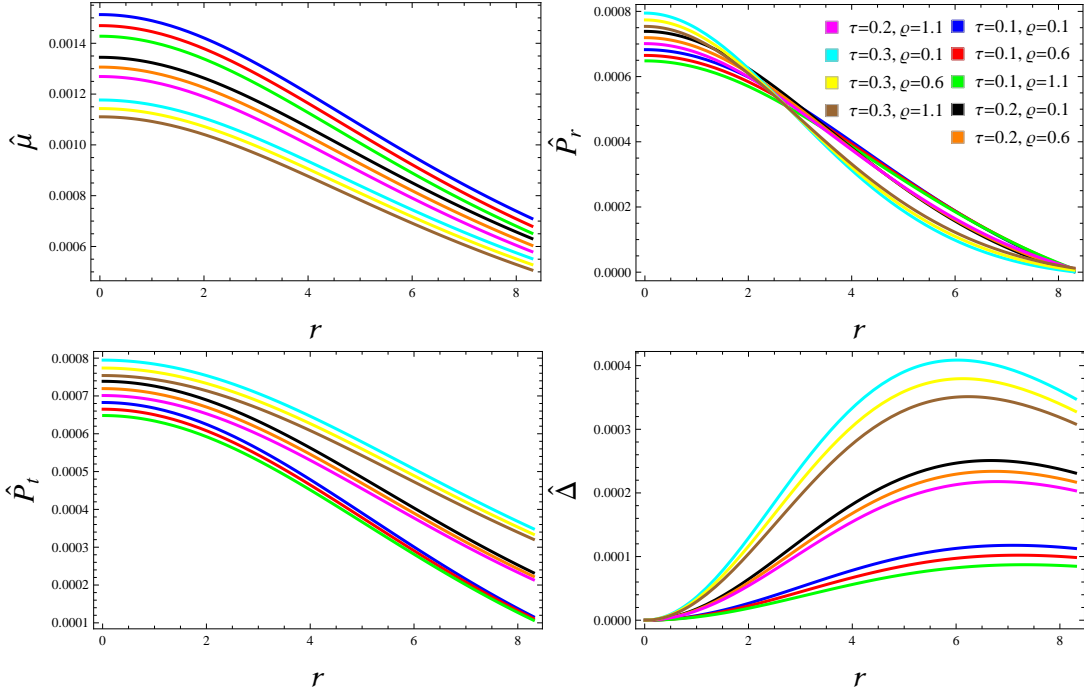


FIG. 2: Fluid parameters for model 1.

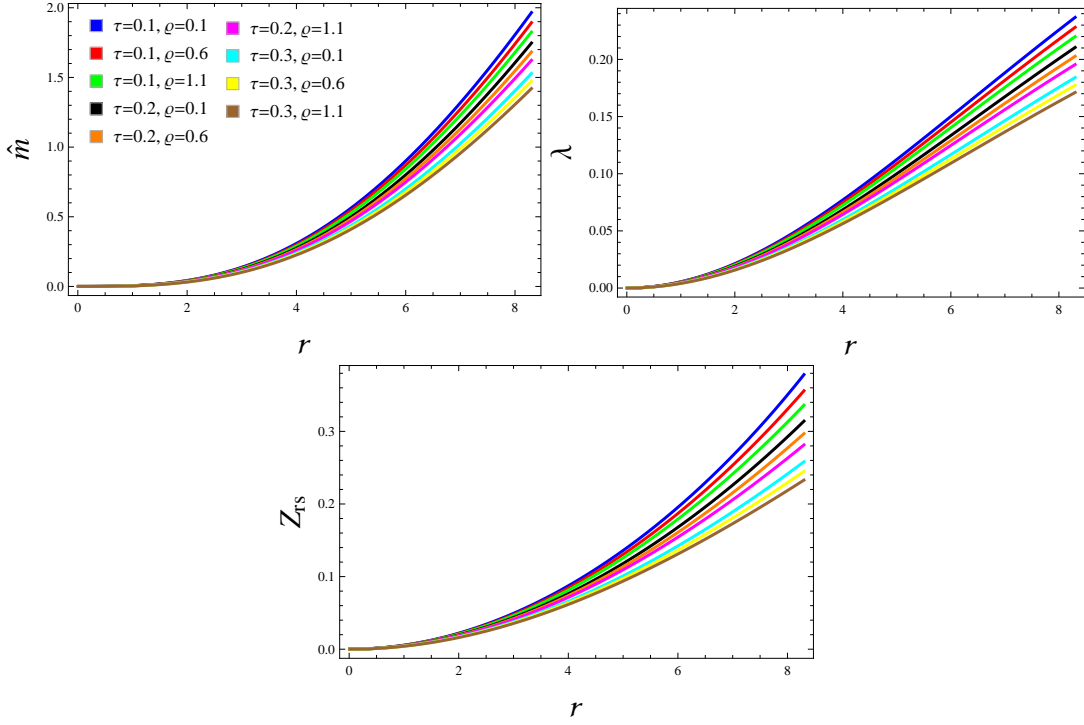


FIG. 3: Physical parameters for model 1.

Combining Eqs.(21), (24) and (47) together, a single equation is obtained in the following

$$\frac{d(r)}{8\pi} \left\{ \frac{p'_1}{r} + \frac{1}{r^2} \right\} - \frac{e^{-p_2}}{8r^2(\varrho^2 + 6\pi\varrho + 8\pi^2)} \times [(3\varrho + 8\pi)rp'_1 + \varrho rp'_2 - 2(\varrho + 4\pi)(e^{p_2} - 1)] = 0, \quad (48)$$

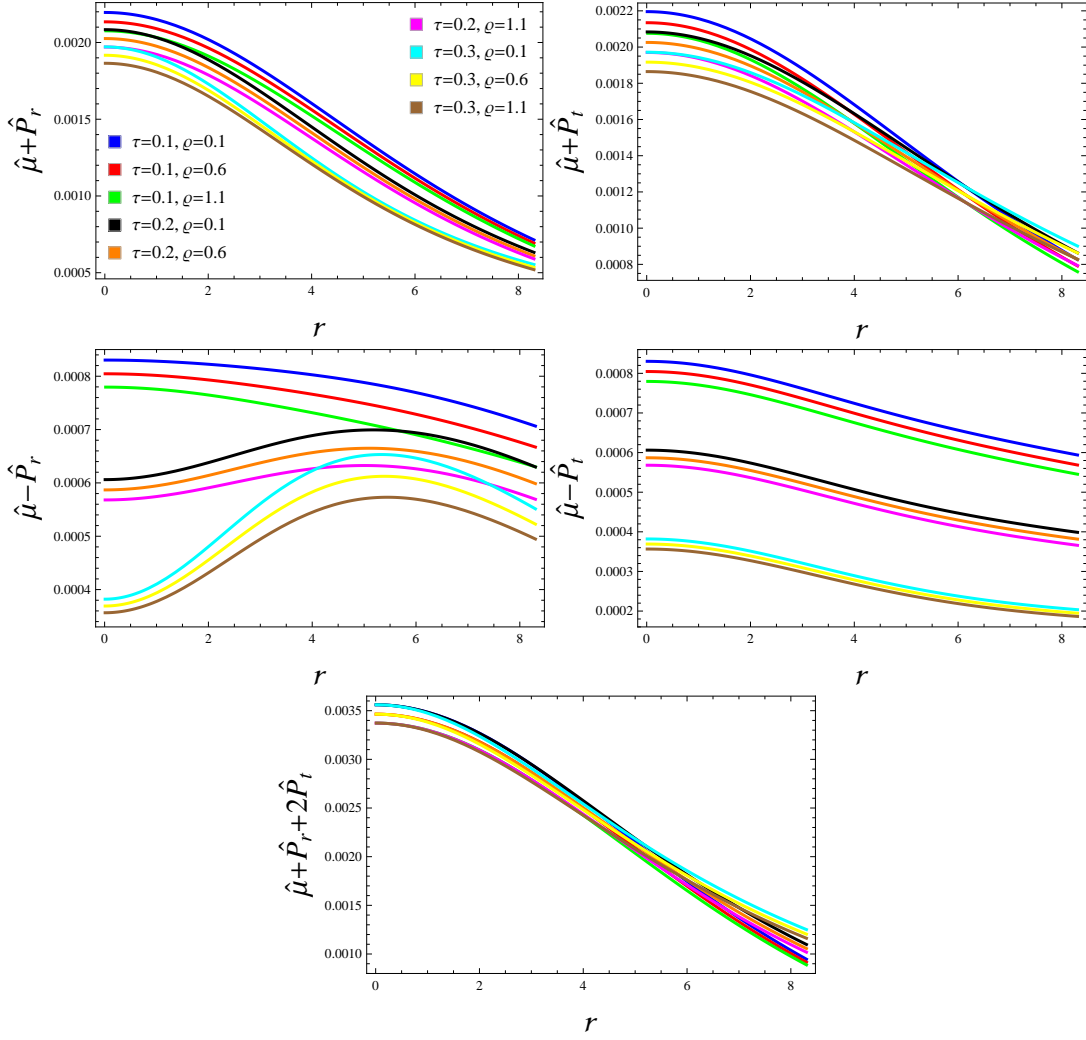


FIG. 4: Energy conditions for model 1.

which becomes when substituting metric components (27) and (28) as

$$\begin{aligned} & \left(\frac{6b_2}{b_2r^2 + 1} + \frac{1}{r^2} \right) d(r) + \frac{6\pi b_2}{(\varrho + 2\pi)(\varrho + 4\pi)\psi^3 (b_2r^2 + 1)^2} \\ & \times [2\pi b_3 - 3(\varrho + 2\pi)\psi + b_2^2 r^4 \{8(\varrho + 3\pi)\psi + 7(3\varrho + 8\pi)b_3\} \\ & + 2b_2r^2 \{(3\varrho + 11\pi)b_3 - (5\varrho + 9\pi)\psi\}] = 0. \end{aligned} \quad (49)$$

The explicit expression for the deformation function can be easily obtained for the above equation as

$$\begin{aligned} d(r) = & \frac{-6\pi b_2 r^2}{(\varrho + 2\pi)(\varrho + 4\pi)\psi^3 (b_2r^2 + 1) (7b_2r^2 + 1)} [2\pi b_3 + b_2^2 r^4 \{8(\varrho + 3\pi)\psi \\ & + 7(3\varrho + 8\pi)b_3\} - 3(\varrho + 2\pi)\psi + 2b_2r^2 \{(3\varrho + 11\pi)b_3 - (5\varrho + 9\pi)\psi\}]. \end{aligned} \quad (50)$$

Equation (16) thus produces in conjunction with (50) as

$$\begin{aligned} e^{p_2(r)} = & \frac{2(b_2r^2 + 1) \sqrt{4b_2r^2 + 1}}{(2 - b_2r^2) \sqrt{4b_2r^2 + 1} - 3b_2b_3r^2} - \frac{6\pi\tau b_2r^2 (7b_2r^2 + 1)^{-1}}{(\varrho + 2\pi)(\varrho + 4\pi)\psi^3 (b_2r^2 + 1)} \\ & \times [2\pi b_3 + b_2^2 r^4 \{8(\varrho + 3\pi)\psi + 7(3\varrho + 8\pi)b_3\} - 3(\varrho + 2\pi)\psi + 2b_2r^2 \\ & \times \{(3\varrho + 11\pi)b_3 - (5\varrho + 9\pi)\psi\}]. \end{aligned} \quad (51)$$

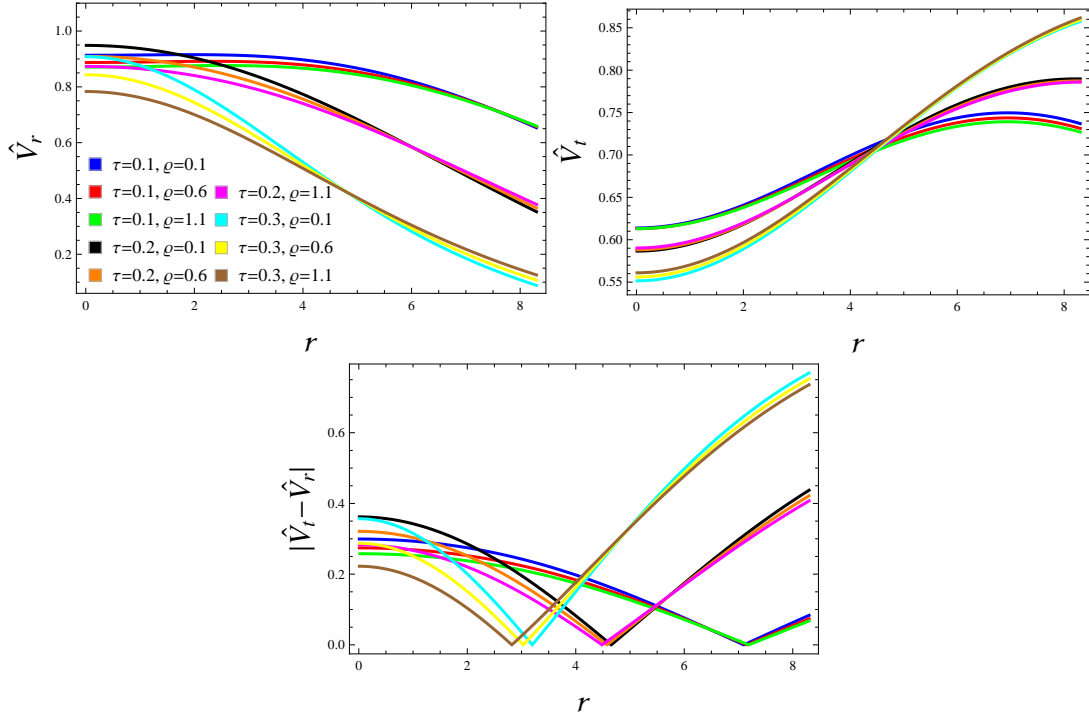
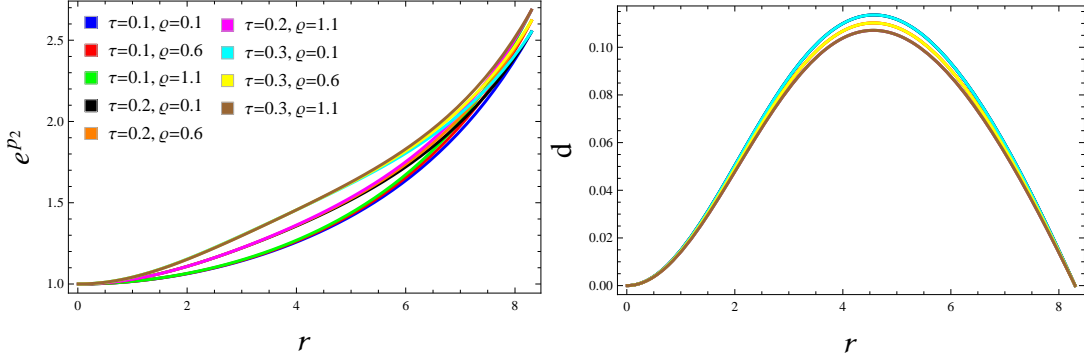


FIG. 5: Stability for model 1.

FIG. 6: Modified g_{rr} potential and deformation function for model 2.

Equations (25) and (26) can now be used to construct the final form of effective fluid parameters. The values of parameters ρ and τ remain the same as we choose earlier to discuss model 1. However, in this case, b_2 is chosen as 0.002 km^{-2} . In Figure 6, we discuss the behavior of modified g_{rr} component and deformation function (expressed in the last two equations), and find them well-behaved. From the right plot, we see that the function $d(r)$ reaches a maximum of 0.11 at $r = 4.5$ and null both at the core and spherical interface for all choices of parameters. In Figure 7, we also check the trend of fluid parameters and anisotropy in the pressure. We observe that effective density corresponding to model 2 exhibits same profile as of model 1 but only near the center of a star. This relation becomes opposite as we move towards the boundary. The same observation is carried out regarding the radial component of pressure. As the anisotropy is concerned, this factor rapidly decreases near the interface for this resulting model as compared to the previous one.

In the stellar interior, the mass function and its dependent properties are also investigated in Figure 8. We find the less massive system in this case when comparing numerical values with those of model 1 for all values of ρ and τ . The existence of usual matter in a celestial body is also needed to explore because this helps in existing the compact stars physically. For this, we plot the energy bounds in Figure 9 and find all of them lying in positive range, ultimately showing the viability. Lastly, Figure 10 exhibits the plots of stability checkers which are consistent with their criteria, hence, our model 2 is stable.

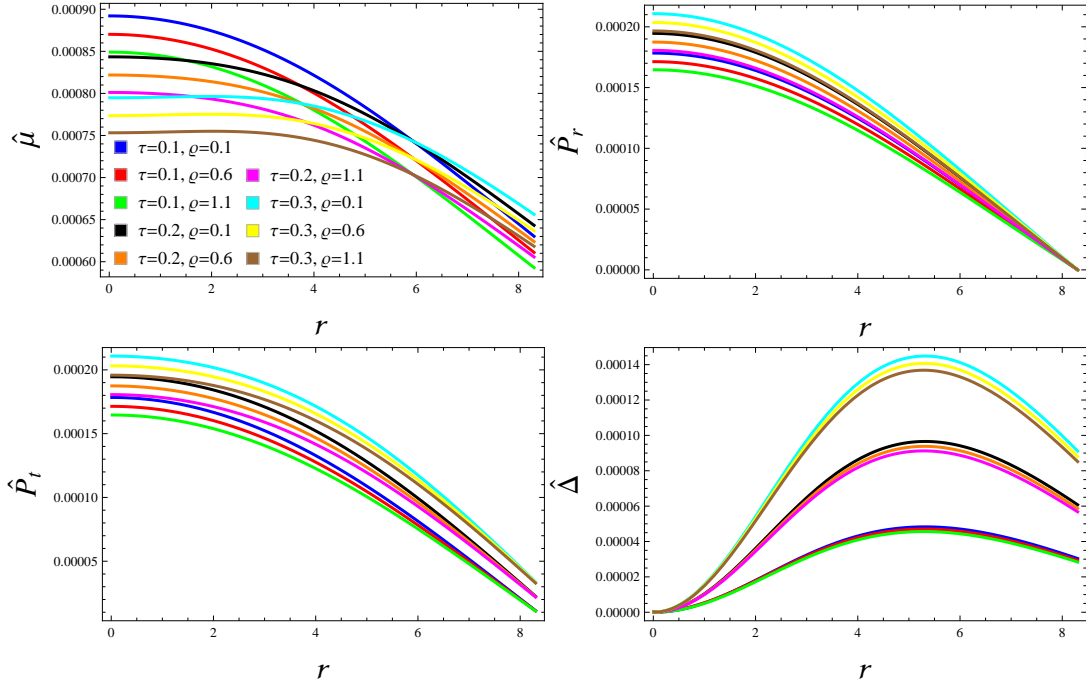


FIG. 7: Fluid parameters for model 2.

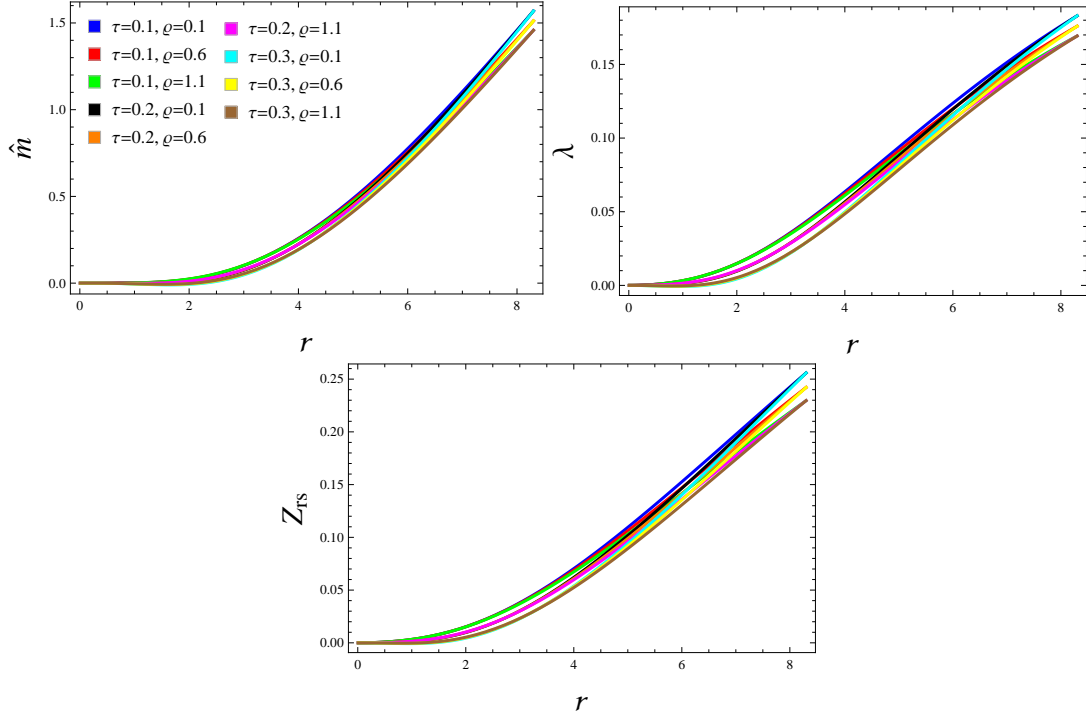


FIG. 8: Physical parameters for model 2.

C. Advantages of Our Approach over Existing Methods: A Brief Summary

To understand how this approach improves upon existing methods for modeling anisotropic structures in $f(R, T)$ gravity, it is essential to highlight several key aspects that differentiate this work from previous studies. Firstly, this methodology employs a gravitational decoupling approach that allows for a more nuanced interaction between fluid

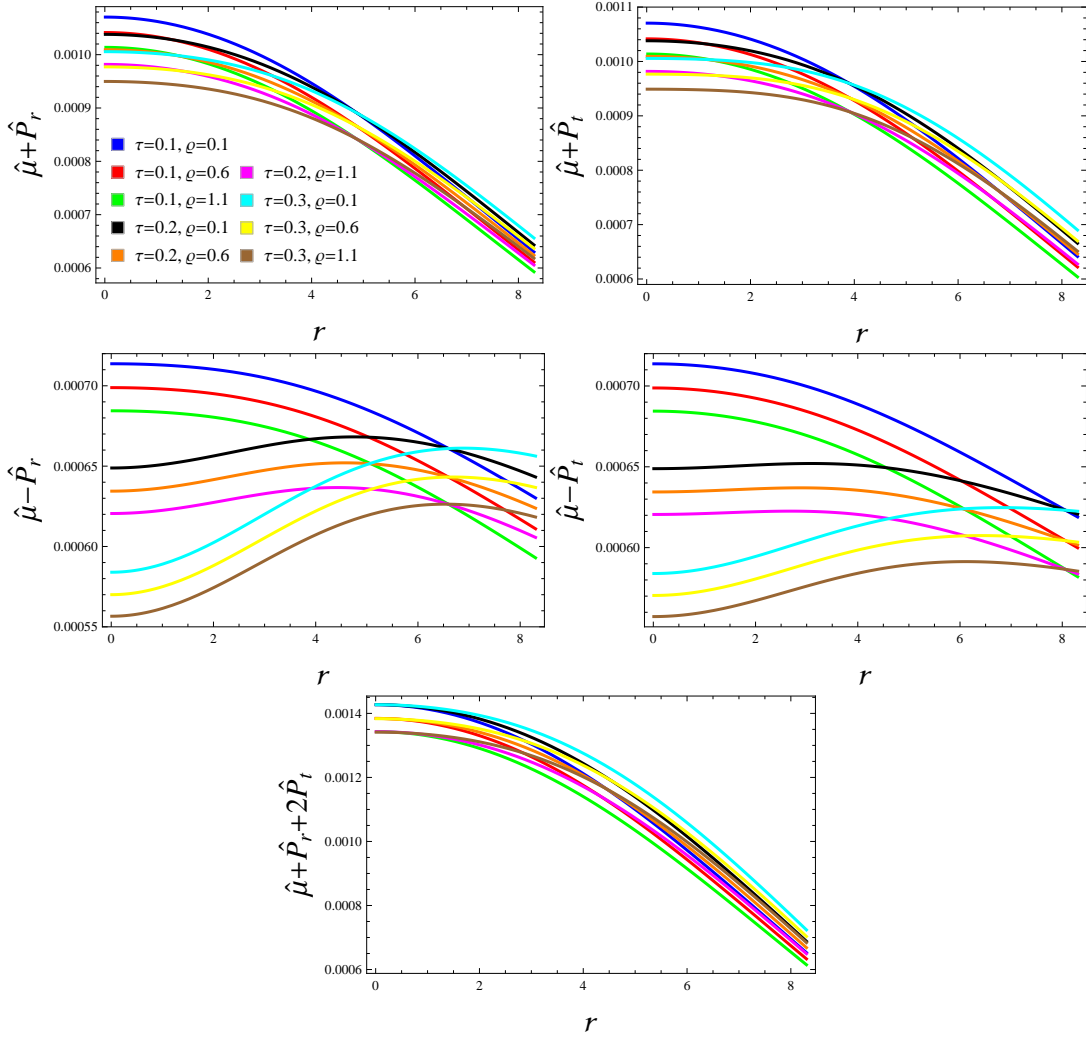


FIG. 9: Energy conditions for model 2.

dynamics and geometry. Traditional models often rely on isotropic fluid configurations as a starting point, which can limit the exploration of anisotropic behaviors. By deriving multiple anisotropic analogs from an established isotropic model, a framework is introduced that not only retains the foundational characteristics of isotropic models but also systematically incorporates the complexities introduced by anisotropic sources. This duality enhances the robustness of the resulting field equations, enabling a comprehensive analysis of the matter distribution within compact objects.

Secondly, the introduction of a new matter source to induce anisotropic behavior is a significant advancement. Existing models frequently assume predefined equations of state or specific forms of matter distribution, which may not accurately reflect the physical conditions within compact stars. In contrast, this approach allows for greater flexibility in modeling the internal structure of these objects by accommodating various forms of anisotropic pressures and densities. This adaptability is particularly crucial in astrophysical contexts where the nature of matter can be highly variable and influenced by factors such as density fluctuations and phase transitions. Moreover, the use of Heintzmann's ansatz and specific constraints on additional gravitating sources provides a structured method to tackle the complexities arising from anisotropic configurations. This approach facilitates a clearer delineation between different fluid sources, allowing for a more straightforward interpretation of the resulting equations. The ability to split the field equations into two distinct sets not only simplifies the analysis but also enhances the clarity with which we can understand the physical implications of anisotropy in stellar structures. Finally, a thorough assessment of the physical validity of the models has been conducted using observational data from a specific star candidate, LMC X-4. This empirical grounding is crucial as it ensures that the theoretical advancements made through this approach are not merely abstract but are aligned with real astrophysical phenomena. By demonstrating that the developed models adhere to established acceptability criteria under certain parametric values, a compelling evidence has been provided

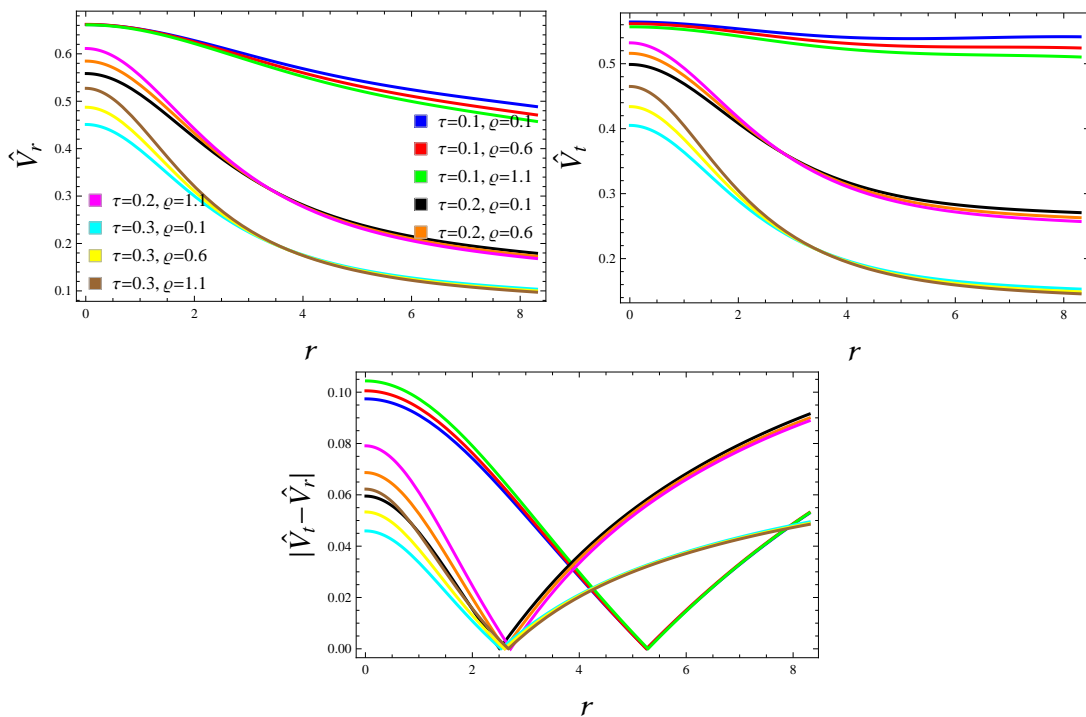


FIG. 10: Stability for model 2.

that this method offers practical improvements over existing modeling techniques.

In addressing the limitations of stability tests, it is essential to consider both causality conditions and Herrera's cracking criteria. Causality conditions ensure that the propagation of signals does not exceed the speed of light, which is a fundamental aspect of relativistic theories. Furthermore, Herrera's cracking criteria provide a framework for analyzing the stability of anisotropic configurations, particularly in relation to the onset of instabilities such as cracking or fragmentation within the matter distribution. We acknowledge that not all configurations may satisfy Herrera's criteria across all parameter spaces. This limitation suggests that further investigation is needed to explore the stability of our models under varying conditions and to identify potential regions where instabilities could arise. In addition to these considerations, we also recognize the importance of other stability criteria that may be relevant in our context. For instance, examining the effects of perturbations on our solutions could reveal additional insights into their stability. However, this is not performed in our analysis at this time.

Inflation potentials play a crucial role in the context of cosmological models, particularly in explaining the dynamics of the early universe. In essence, inflation refers to a rapid exponential expansion that occurred shortly after the Big Bang, driven by a scalar field known as the inflaton. The potential energy associated with this field dictates the rate of expansion and the dynamics of the universe during this phase. In relation to our model derived from isotropic fluid dynamics, inflation potentials are significant because they provide a framework for understanding how anisotropic behavior can emerge from an initially isotropic configuration. By introducing a new matter source that influences the gravitational dynamics, we can explore how these potentials affect the stability and evolution of anisotropic models. Moreover, the relationship between inflation potentials and our model is evident in how these potentials can influence the effective equations governing fluid-geometry interactions. The anisotropic configurations we develop can be viewed as modifications to standard cosmological models, incorporating effects from inflationary dynamics.

VII. CONCLUDING REMARKS

In this study, we have developed various anisotropic analogs of a well-known isotropic ansatz within the framework of the model $f(R, T) = R + 2\varrho T$. Initially, we assumed a spherical configuration filled with isotropic perfect fluid, which transitions to the anisotropic state upon introducing an additional source at the action level. The modified action (1) consequently leads to field equations that incorporate the influences of both the original isotropic configuration and the additional sources within the modified theory. To manage these equations effectively, we employed the MGD strategy to split them into two distinct sets. The first set of equations was addressed by adopting the Heintzmann's

solution as follows

$$e^{p_1(r)} = b_1^2 (b_2 r^2 + 1)^3 ,$$

$$e^{p_2(r)} = \frac{2 (b_2 r^2 + 1) \sqrt{4b_2 r^2 + 1}}{(2 - b_2 r^2) \sqrt{4b_2 r^2 + 1} - 3b_2 b_3 r^2} ,$$

and derived the constant triplet (b_1, b_2, b_3) by applying smooth matching criteria at the junction $\Sigma : r = \bar{R}$. Additionally, the Φ -sector described by Eqs.(22)-(24) involved four unknowns that required determination. Subsequently, we imposed distinct constraints on $\Phi_{\sigma\omega}$, leading to the development of two distinct solutions. These solutions were then combined via the parameter τ to incorporate contributions from both sources, resulting in the generation of novel anisotropic analogs.

We have further explored the criteria for acceptability which ensure that the derived solution must align with these conditions if it is claimed to be physically relevant. The physical attributes for all constructed models have been visually interpreted for specific parameter values, such as $\varrho = 0.1, 0.6, 1.1$ and $\tau = 0.1, 0.2, 0.3$. Our observations reveal consistent behavior of fluid triplet across all parametric combinations. Also, the anisotropic factor has been noticed to be an increasing function of r . The mass functions were plotted for every developed model to see which condition on the additional fluid source produce more dense interior. We observe model 1 to be more dense in comparison with the other model. Moreover, some other factors have also been demonstrated to be consistent with the observational data. The energy bounds were seen to be positive, indicated the viability of all models. Finally, occurrence of cracking has not been observed in any case, hence, models 1, 2 and 3 are stable. Furthermore, when compared to prior studies within $f(R, T)$ gravity, our models offer unique insights into the physical validity of anisotropic configurations. Previous works have explored various aspects of anisotropic stars and their stability under different gravitational frameworks; however, our approach specifically emphasizes the transformation of isotropic solutions into anisotropic ones while maintaining consistency with the underlying physics. We must highlight here that the anisotropic Heintzmann's extensions are more suitable as compared to those of Buchdahl's solution [74]. We can find all these results in GR when putting $\varrho = 0$.

Data Availability Statement: This manuscript has no associated data.

-
- [1] Capozziello, S. et al.: *Class. Quantum Grav.* **25**(2008) 085004.
 - [2] Nojiri, S. et al.: *Phys. Lett. B* **681**(2009)74.
 - [3] de Felice, A. and Tsujikawa, S.: *Living Rev. Relativ.* **13**(2010)3.
 - [4] Nojiri, S. and Odintsov, S.D.: *Phys. Rep.* **505**(2011)59.
 - [5] Sharif, M. and Kausar, H.R.: *J. Cosmol. Astropart. Phys.* **07**(2011)022.
 - [6] Astashenok, A.V., Capozziello, S., Odintsov, S.D. and Oikonomou, V.K.: *Phys. Lett. B* **816**(2021)136222.
 - [7] Astashenok, A.V., Capozziello, S. and Odintsov, S.D.: *J. Cosmol. Astropart. Phys.* **12**(2013)040.
 - [8] Astashenok, A.V., Odintsov, S.D. and Oikonomou, V.K.: *Phys. Rev. D* **106**(2022)124010.
 - [9] Bertolami, O. et al.: *Phys. Rev. D* **75**(2007)104016.
 - [10] Naseer, T., Sharif, M., Fatima, A. and Manzoor, S.: *Chin. J. Phys.* **86**(2023)350.
 - [11] Harko, T. et al.: *Phys. Rev. D* **84**(2011)024020.
 - [12] Deng, X.M. and Xie, Y.: *Int. J. Theor. Phys.* **54**(2015)1739.
 - [13] Houndjo, M.J.S.: *Int. J. Mod. Phys. D* **21**(2012)1250003.
 - [14] Das, A. et al.: *Phys. Rev. D* **95**(2017)124011.
 - [15] Maurya, S.K., Banerjee, A. and Tello-Ortiz, F.: *Phys. Dark Universe* **27**(2020)100438.
 - [16] Singh, K.N. et al.: *Phys. Dark Universe* **30**(2020)100620.
 - [17] Maurya, S.K.: *Phys. Dark Universe* **30**(2020)100640.
 - [18] Rej, P., Bhar, Piyali. and Govender, M.: *Eur. Phys. J. C* **81**(2021)316.
 - [19] Kaur, S., Maurya, S.K., Shukla, S. and Nag, R.: *Chin. J. Phys.* **77**(2022)2854.
 - [20] Sharif, M. and Naseer, T.: *Eur. Phys. J. Plus* **137**(2022)1304.
 - [21] Sharif, M. and Naseer, T.: *Phys. Scr.* **98**(2023)115012.
 - [22] Maurya, S.K., Singh, K.N., Govender, M. and Ray, S.: *Fortschr. Phys.* **71**(2023)2300023.
 - [23] Sharif, M. and Naseer, T.: *Ann. Phys.* **459**(2023)169527.
 - [24] Feng, Y. et al.: *Phys. Scr.* **99**(2024)085034.
 - [25] Demir, E. et al.: *Chin. J. Phys.* **91**(2024)299.
 - [26] Zubair, M., Waheed, S. and Ahmad, Y.: *Eur. Phys. J. C* **76**(2016)444.
 - [27] Das, A., Rahaman, F., Guha, B.K. and Ray, S.: *Eur. Phys. J. C* **76**(2016)654.
 - [28] Moraes, P.H.R.S., Correa, R.A.C. and Lobato, R.V.: *J. Cosmol. Astropart. Phys.* **07**(2017)029.
 - [29] Zaregonbadi, R. et al.: *Phys. Rev. D* **94**(2016)084052.

- [30] Buniy, R.V., Berera, A. and Kephart, T.W.: Phys. Rev. D **73**(2006)063529.
- [31] Saadeh, D., Feeney, S.M., Pontzen, A., Peiris, H.V. and McEwen, J.D.: Phys. Rev. Lett. **117**(2016)131302.
- [32] Mishra, B., Ray, P.P. and Myrzakulov, R.: Eur. Phys. J. C **79**(2019)34.
- [33] Sokolov, A.I.: Sov. Phys.-JETP **52**(1980)575.
- [34] Weber, F.: J. Phys. G: Nucl. Part. Phys. **25**(1999)R195.
- [35] Sawyer, R.F.: Phys. Rev. Lett. **29**(1972)382.
- [36] Schunck, F.E. and Mielke, E.W.: Class. Quantum Grav. **20**(2003)R301.
- [37] Rahaman, F., Ray, S., Jafry, A.K. and Chakraborty, K.: Phys. Rev. D **82**(2010)104055.
- [38] Maurya, S.K., Mishra, B., Ray, S. and Nag, R.: Chin. Phys. C **46**(2022)105105.
- [39] Migkas, K. and Reiprich, T.H.: Astron. Astrophys. **611**(2018)A50.
- [40] Migkas, K., Schellenberger, G., Reiprich, T.H., Pacaud, F., Ramos-Ceja, M.E. and Lovisari, L.: Astron. Astrophys. **636**(2020)A15.
- [41] Ovalle, J.: Phys. Rev. D **95**(2017)104019.
- [42] Ovalle, J.: Phys. Lett. B **788**(2019)213.
- [43] Naseer, T.: Astropart. Phys. **166**(2025)103073.
- [44] Ovalle, J. et al.: Eur. Phys. J. C **78**(2018)960.
- [45] Sharif, M. and Sadiq, S.: Eur. Phys. J. C **78**(2018)410.
- [46] Sharif, M. and Waseem, A.: Ann. Phys. **405**(2019)14.
- [47] Gabbanelli, L., Rincón, Á. and Rubio, C.: Eur. Phys. J. C **78**(2018)370.
- [48] Estrada, M. and Tello-Ortiz, F.: Eur. Phys. J. Plus **133**(2018)453.
- [49] Hensh, S. and Stuchlík, Z.: Eur. Phys. J. C **79**(2019)834.
- [50] Sharif, M. and Ama-Tul-Mughani, Q.: Mod. Phys. Lett. A **35**(2020)2050091.
- [51] Sharif, M. and Naseer, T.: Chin. J. Phys. **73**(2021)179.
- [52] Sharif, M. and Naseer, T.: Int. J. Mod. Phys. D **31**(2022)2240017.
- [53] Ashmita, Sarkar, P. and Das, P.K.: Int. J. Mod. Phys. D **31**(2022)2250120.
- [54] Kaur, S., Maurya, S.K., Shukla, S. and Nag, R.: Chin. J. Phys. **77**(2022)2854.
- [55] Sharif, M. and Naseer, T.: Class. Quantum Grav. **40**(2023)035009.
- [56] Naseer, T. and Sharif, M.: Fortschr. Phys. **71**(2023)2300004.
- [57] Maurya, S.K. and Tello-Ortiz, F.: Phys. Dark Universe **27**(2020)100442.
- [58] Maurya, S.K., Mishra, B., Ray, S. and Nag, R.: Chin. Phys. C **46**(2022)105105.
- [59] Heintzmann, H.: Z. Phys. **228**(1969)489.
- [60] Delgaty, M.S.R. and Lake, K.: Comput. Phys. Commun. **115**(1998)395.
- [61] Gangopadhyay, T., Ray, S., Xiang-Dong, L., Jishnu, D. and Mira, D.: Mon. Not. R. Astron. Soc. **431**(2013)3216.
- [62] Delgaty, M.S.R. and Lake, K.: Comput. Phys. Commun. **115**(1998)395.
- [63] Ivanov, B.V.: Eur. Phys. J. C **77**(2017)738.
- [64] Sharif, M. and Naseer, T.: Phys. Dark Universe **42**(2023)101324.
- [65] Misner, C.W. and Sharp, D.H.: Phys. Rev. **136**(1964)B571.
- [66] Buchdahl, H.A.: Phys. Rev. **116**(1959)1027.
- [67] Ivanov, B.V.: Phys. Rev. D **65**(2002)104011.
- [68] Naseer, T.: Phys. Dark Universe **46**(2024)101663.
- [69] Feng, Y. et al.: Chin. J. Phys. **90**(2024)372.
- [70] Abreu, H., Hernandez, H. and Nunez, L.A.: Class. Quantum Grav. **24**(2007)4631.
- [71] Herrera, L.: Phys. Lett. A **165**(1992)206.
- [72] Heras, C.L. and León, P.: Fortschr. Phys. **66**(2018)1800036.
- [73] Graterol, R.P.: Eur. Phys. J. Plus **133**(2018)244.
- [74] Naseer, T. and Sharif, M.: Phys. Scr. **99**(2024)035001.